Journal of Particle Science and Technology 1 (2015) 225-240

Journal of Particle Science and Technology

J | P | S | T

jpst.irost.ir

Effects of brownian motion and thermophoresis on MHD mixed convection stagnation-point flow of a nanofluid toward a stretching vertical sheet in porous medium

Aboutaleb Ghadami Jadval Ghadam*[1], Abed Moradi[2]

[1]*Department of Chemical Engineering, Yasooj Branch, Islamic Azad University, Yasooj, Iran*

[2]*Young Researchers Club, Yasooj Branch, Islamic Azad University, Yasooj, Iran*

HIGHLIGHTS

- Two-dimensional mixed convection MHD boundary layer of stagnation-point flow over a stretching vertical plate in porous medium filled with a nanofluid was investigated.
- The governing partial differential equations were converted to ordinary differential equations.
- The volume fraction of nanoparticles may be a key parameter for studying the effect of nanoparticles on flow fields and temperature distributions.

GRAPHICAL ABSTRACT

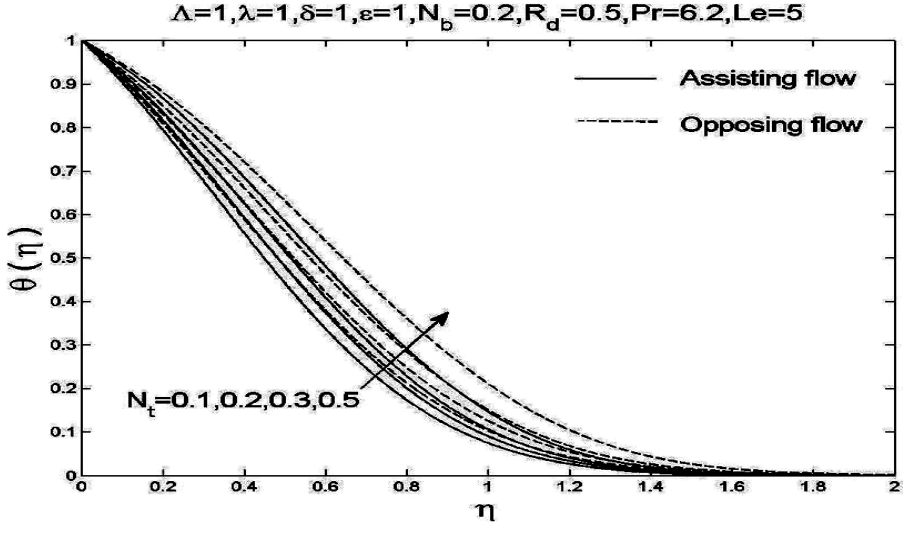

ARTICLE INFO

Article history:
Received 21 March 2016
Received in revised form
29 April 2016
Accepted 05 May 2016

Keywords:
MHD mixed convection
Stagnation-point flow
Stretching vertical plate
Nanofluid
Porous medium
Brownian motion

ABSTRACT

This article deals with the study of the two-dimensional mixed convection magnetohydrodynamic (MHD) boundary layer of stagnation-point flow over a stretching vertical plate in porous medium filled with a nanofluid. The model used for the nanofluid incorporates the effects of Brownian motion and thermophoresis in the presence of thermal radiation. The skin-friction coefficient, Nusselt number and local Sherwood number as well as the velocity, temperature and concentration profiles for some values of the governing parameters were presented graphically and discussed in detail for both the cases of assisting and opposing flows. It was observed that, the magnitude of the reduced Nusselt number decreases with the increases in the Brownian motion and thermophoresis effects for both cases of buoyant assisting and opposing flows. In addition to, the local Sherwood number increases by increasing the Brownian motion in both cases of buoyant assisting and opposing flows. A similar effect on the local Sherwood number was observed when thermophoresis effects decreases.

*Corresponding author Tel: +98 9171458176
E-mail address: ghadami@iauyasooj.ac.ir; aghadami80@gmail.com

1. Introduction

Stagnation-point flow, describing the fluid motion near the stagnation region of a solid surface exists in both cases of a fixed or moving body in a fluid. Hiemenz [1] was the first to study the two-dimensional stagnation point flow, and obtained an exact similarity solution of the governing Navier–Stokes equations. Eckert [2] extended this work by including the energy equation and obtained an exact similar solution for the thermal field. In the recent decade, Dinarvand [3] considered the off-centered stagnation flow towards a rotating disc by means of HAM. Since then many investigators have considered various aspects of such flow, and obtained closed form analytical as well as numerical solutions. The flow and heat transfer due to a stretching surface in a viscous fluid is of great practical interest because it occurs in a number of engineering processes i.e. in the polymer industry when a polymer sheet is extruded continuously from a die, with a tacit assumption that the sheet is inextensible. During its manufacturing process a stretched sheet interacts with the ambient fluid both thermally and mechanically. Convective heat transfer in porous media has been a subject of great interest for the last several decades. The research activities in this field has been accelerated because of a broad range of applications in various disciplines, such as geophysical, thermal and insulating engineering, solar power collector, cooling of electronic systems, crystal growth in liquids, chemical catalytic reactors, petroleum reservoirs, nuclear waste repositories, post-accident heat removal from pebble-bed nuclear reactors, etc. The state of-the-art has been very well summarised in the recent books by Nield and Bejan [4], Ingham and Pop [5, 6] and Bejan et al. [7]. The study of magnetic field effects has important applications in physics and engineering. There have been several recent studies on the effect of the magnetic field on the flow and heat transfer problems. Ece [8] investigated the similarity analysis for the laminar free convection boundary layer flow in the presence of a transverse magnetic field over a vertical down-pointing cone with mixed thermal boundary conditions. He determined the boundary layer velocity and temperature profiles numerically for various values of the magnetic parameter and the Prandtl number. Dinarvand et al. [9] examined the unsteady laminar MHD flow near forward stagnation point of an impulsively rotating and translating sphere in presence of buoyancy forces. Also, he [10] studied the boundary-layer flow about a heated and rotating down-pointing vertical cone in the presence of a transverse magnetic field. The effect of thermal radiation on the flow and heat transfer have not been provided in the most investigations. The effect of radiation on MHD flow and heat transfer problem have become more important industrially. At high operating temperature, radiation effect can be quite significant. Many process in engineering areas occur at high temperature and a knowledge of radiation heat transfer becomes very important for design of reliable equipment, nuclear plants, gas turbines and various propulsion devices or aircraft, missiles, satellites and space vehicles. Hayat et al. [11] studied a two dimensional mixed convection boundary layer MHD stagnation point flow through a porous medium bounded by a stretching vertical plate with thermal radiation. Das [12] discussed the effect of thermal radiation on MHD slip flow over a flat plate with variable fluid properties. A nanofluid is a new class of heat transfer fluids that contain a base fluid and nanoparticles. The use of additives is a technique applied to enhance the heat transfer performance of base fluids. The thermal conductivity of the ordinary heat transfer fluids is not adequate to meet today's cooling rate requirements. Nanofluids have been shown to increase the thermal conductivity and convective heat transfer performance of the base liquids. Choi [13] seems to be the first who used the term nanofluids to refer to the fluid with suspended nanoparticles. Choi et al. [14] showed that the addition of a small amount (less than 1% by volume) of nanoparticles to conventional heat transfer liquids increased the thermal conductivity of the fluid up to approximately two times. One of the possible mechanisms for anomalous increase in the thermal conductivity of nanofluids is the Brownian motions of the nanoparticles inside the base fluids. A variety of nuclear reactor designs featured by enhanced safety and improved economics are being proposed by the nuclear power industry around the world to more realistically solve the future energy supply shortfall. Nanofluid coolants showing an improved thermal performance are being considered as a new key technology to secure nuclear safety and economics. Nanofluids are suspensions of nanoparticles in fluids that show significant enhancement of their properties at modest nanoparticle concentrations. Many of the publications on nanofluids are about understanding their behavior so that they can be utilized where straight heat transfer enhancement is paramount as in many industrial applications, nuclear reactors, transportation, electronics as well as biomedicine and food. Magnetic nanofluid is a unique material that has both the liquid and magnetic properties. Many of the physical properties of these fluids can be tuned by varying

model system for fundamental studies. As the magnetic nanofluids are easy to manipulate with an external magnetic field, they have been used for a variety of studies. Brownian diffusion and thermophoresis are important slip mechanisms in nanofluids. Many researchers have investigated different aspects of nanofluids. Thermophysical properties of nanofluids such as thermal conductivity, thermal diffusivity, and viscosity of nanofluids have been studied by Kang et al. [15], Velagapudi et al. [16], Turgut et al. [17], Rudyak et al. [18] Murugesan et al. [19], Tiwari and Das [20], and Nayak et al. [21]. Ahmad and Pop [22] examined the mixed convection boundary layer flow past a vertical flat plate embedded in a porous medium filled with nanofluids. Dinarvand et al. [23] studied Mixed convective boundary layer flow of a nanofluid over a vertical circular cylinder. The two-dimensional boundary layer flow of a nanofluid past a stretching sheet in the presence of magnetic field intensity and the thermal radiation was studied by Gbadeyan and Olanrewaju [24]. Very recently, Dinarvand et al. [25] examined the steady three-dimensional stagnation point flow of a nanofluid past a circular cylinder with sinusoidal radius variation. Thermophoresis is a phenomenon, which causes small particles to be driven away from a hot surface and tower a cold one. Small particles, such as dust, when suspended in a gas with a temperature gradient, experience a force in the direction opposite to the temperature gradient. This phenomenon has many practical applications in removing small particles from gas particle trajectories from combustion devices, and studying the particulate material deposition turbine blades. For more detail on the topic, the readers may consult the studies [26-31]. Das examined [32] the Effects of thermophoresis and thermal radiation on MHD mixed convective heat and mass transfer flow. Very recently, Kuznetsov and Nield [33] have examined the influence of nanoparticles on natural convection boundary-layer flow past a vertical plate, using a model in which Brownian motion and thermophoresis are accounted for. The authors have assumed the simplest possible boundary conditions, namely those in which both the temperature and the nanoparticle fraction are constant along the wall. Further, Nield and Kuznetsov [34] have studied the Cheng and Minkowycz [35] problem of natural convection past a vertical plate, in a porous medium saturated by a nanofluid. The model used for the nanofluid incorporates the effects of Brownian motion and thermophoresis. For the porous medium the Darcy model has been employed. The Boungiorno [36] model has recently been used by Kuznetsov and Nield [33] to study the natural convec tive flow of a nanofluid over a vertical plate. Their similarity analysis identified four parameters governing the transport process, namely a Lewis number Le, a buoyancy-ratio number Nr, a Brownian motion number Nb, and a thermophoresis number Nt. Also, the boundary layer flow of a nanofluid past a stretching sheet is considered by Khan and Pop [37] using Buongiorno's model. The main goal of the present study is to investigate the two-dimensional mixed convection magnetohydrodynamic (MHD) boundary layer of stagnation-point flow over a stretching vertical plate in porous medium filled with a nanofluid in the presence of thermal radiation. Combined effects of heat and mass transfer in presence of Brownian motion and thermophoresis are also taken into account. Using a similarity transform the Navier–Stokes equations have been reduced to a set of nonlinear ordinary differential equations. The resulting non linear system has been solved numerically using the Runge–Kutta–Fehlberg method with a shooting technique. The effects of embedded parameters on fluid velocity, temperature and particle concentration have been shown graphically. It is hoped that the results obtained will not only provide useful information for applications, but also serve as a complement to the previous studies.

2. Problem statement and mathematical formulation

Consider the steady flow and heat transfer of an incompressible viscous nanofluid flow near the magnetohydrodnamic stagnation-point of a stretching vertical plate in a porous medium Two equal and opposite forces are applied along the x-axis so the surface (at) is stretched by keeping the origin fixed in a MHD viscous fluid of constant ambient temperature (see Figure-1). A uniform magnetic field of strength B_0 is applied in the positive direction of y-axis.The ambient uniform temperature and concentration of fluid is T_∞ and C_∞ , where the body surface is kept at a constant temperature T_w and constant concentration C_w , respectively. The stretching velocity $u_w(x)$ and the ambient fluid velocity $U(x)$ are assumed to vary linearly from the stagnation point as $u_w(x)= cx$ and $U(x)= ax$, where a and c are positive constants. Moreover, the effects of Brownian motion and thermophoresis on flow and heat transfer are also considered. The governing equations for conservation of mass, momentum, temperature and nanoparticles equations for nanofluids can be expressed as, (see Khan and Pop [37])

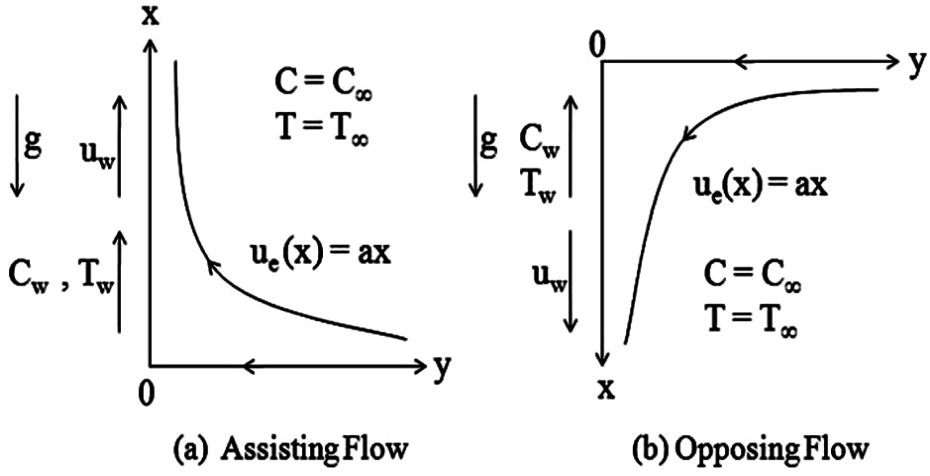

Fig. 1. Physical model and coordinate system.

$$\frac{\partial u}{\partial x}+\frac{\partial v}{\partial y}=0, \tag{1}$$

$$u\frac{\partial u}{\partial x}+v\frac{\partial u}{\partial y}=U\frac{dU}{dx}+\nu\frac{\partial^2 u}{\partial y^2}\pm g\beta_T(T-T_\infty)\pm g\beta_c(C-C_\infty)+\frac{\nu}{k}(U-u)+\frac{\sigma B_0^2}{\rho}(U-u), \tag{2}$$

$$u\frac{\partial T}{\partial x}+v\frac{\partial T}{\partial y}=\alpha\left(\frac{\partial^2 T}{\partial x^2}+\frac{\partial^2 T}{\partial y^2}\right)+\tau\left\{D_B\left(\frac{\partial C}{\partial x}\frac{\partial T}{\partial x}+\frac{\partial C}{\partial y}\frac{\partial T}{\partial y}\right)+\frac{D_T}{T_\infty}\left[\left(\frac{\partial T}{\partial x}\right)^2+\left(\frac{\partial T}{\partial y}\right)^2\right]\right\}-\frac{1}{\rho c_P}\frac{\partial q_r}{\partial y}, \tag{3}$$

$$u\frac{\partial C}{\partial x}+v\frac{\partial C}{\partial y}=D_B\left(\frac{\partial^2 C}{\partial x^2}+\frac{\partial^2 C}{\partial y^2}\right)+\frac{D_T}{T_\infty}\left(\frac{\partial^2 T}{\partial x^2}+\frac{\partial^2 T}{\partial y^2}\right), \tag{4}$$

subject to the boundary conditions

$$u=u_w(x)=cx,\quad v=0,\quad T=T_w,\quad c=c_w\quad at\quad y=0, \tag{5}$$

$$u=U(x)=ax,\quad T=T_\infty,\quad c=c_\infty\quad as\quad y\to\infty, \tag{6}$$

Here, u and v are the velocity components along x and y axes, respectively, T is temperature, ρ is the density of base fluid, ν is the kinematic viscosity of the base fluid, α is the thermal diffusivity of the base fluid, σ is the electrical conductivity of the fluid, k is the permeability of the porous medium, g is the gravitational acceleration, β_T is the thermal expansion coefficient, β_c is the coefficient of expansion with concentration, τ is the ratio of nanoparticle heat capacity and the base fluid heat capacity, D_B is the Brownian diffusion coefficient, D_T is the thermophoretic diffusion coefficient, q_r is the radiative heat flux, respectively, the "+ " and " " signs in Eq. (2) respectively correspond to assisting buoyant flow and opposing buoyant flow. The radiative heat flux q_r is described by Roseland approximation such that, ([32] and [41])

$$q_r=-\frac{4\sigma^*}{3k^*}\frac{\partial T^4}{\partial y}, \tag{7}$$

where ó* is the Stefan–Boltzmann constant and k^* is the mean absorption coefficient. We assume that the temperature differences within the flow are sufficiently small so that the T^4 can be expressed as a linear function after using Taylor series to expand T^4 about the free stream temperature T_∞ and neglecting higher-order terms. This result is the following approximation

$$T^4\cong 4T_\infty^3T-3T_\infty^4. \tag{8}$$

From Eqs. (3), (7) and (8) one obtains

$$u\frac{\partial T}{\partial x}+v\frac{\partial T}{\partial y}=\alpha\left(\frac{\partial^2 T}{\partial y^2}\right)+\tau\left[D_B\left(\frac{\partial C}{\partial y}\frac{\partial T}{\partial y}\right)+\frac{D_T}{T_\infty}\left(\frac{\partial T}{\partial y}\right)^2\right]+\frac{16\sigma^*T_\infty^3}{3(\rho c_P)k^*}\frac{\partial^2 T}{\partial y^2}, \tag{9}$$

To obtain similarity solutions for the system of Eqs. (1)–(4), we introduce the following similarity variables, ([28] and [32])

$$\psi=\sqrt{cv}xf(\eta),\qquad \eta=\sqrt{\frac{c}{\nu}}y,\qquad \theta(\eta)=\frac{T-T_\infty}{T_w-T_\infty},\qquad \phi(\eta)=\frac{C-C_\infty}{C_w-C_\infty}, \tag{10}$$

where, ψ is the stream function defined as $u=\partial\psi/\partial y$ and $v=-\partial\psi/\partial x$, which identically satisfy Eq. (1). Using the non-dimensional variables in Eq. (10), Eqs. (2), (3) and (4) reduce to the following ordinary differential equations

$$f'''-f'^2+ff''+\Lambda(\varepsilon-f')+\varepsilon^2\pm\lambda\theta\pm\delta\phi=0, \quad (11)$$

$$(1+\frac{4}{3}R_d)\theta''+Pr\left(N_b\,\theta'\phi'+N_t\,\theta'^2+f\,\theta'\right)=0, \quad (12)$$

$$\phi''+\frac{N_t}{N_b}\theta''+Le\,f\,\phi'=0, \quad (13)$$

where Λ is the constant magnetic/porous medium parameter and ε is The velocity ratio parameter, which are respectively, defined as

$$\Lambda=M^2+\lambda_1=const, \qquad \varepsilon=a/c. \quad (14)$$

The boundary conditions (5) and (6) become

$$\begin{aligned} &f(0)=0, \quad f'(0)=1, \quad f'(\infty)=\varepsilon,\\ &\theta(0)=1, \quad \theta(\infty)=0,\\ &\phi(0)=1, \quad \phi(\infty)=0, \end{aligned} \quad (15)$$

where, primes denote differentiation with respect to η and the constant $\lambda(\geq 0)$ is the buoyancy or mixed convection parameter λ. The mixed convection parameter δ, the solutal buoyancy parameter , the Hartman number M , the porosity parameter λ_1, the Brownian motion parameter N_b , the thermophoresis parameter N_t , the Prandtl number Pr , the Lewis number Le and the radiation parameter R_d are, respectively, defined as

$$\lambda=\frac{Gr}{Re_x^2}, \quad \delta=\frac{Gc}{Re_x^2}, \quad M^2=\frac{\sigma B_0^2}{\rho c}, \quad \lambda_1=\frac{\nu}{Kc}, \quad N_b=\frac{(\rho c_p)_p D_B(C_w-C_\infty)}{(\rho c_p)_f \nu}$$
$$N_t=\frac{(\rho c_p)_p D_T(T_w-T_\infty)}{(\rho c_p)_f T_\infty \nu}, \quad Pr=\frac{\nu}{\alpha}, \quad Le=\frac{\nu}{D_B}, \quad R_d=\frac{4\sigma^* T_\infty^3}{kk_1}. \quad (16)$$

Here, the local Grashof number Gr , the local solutal Grashof number Gc , the local Reynold number Re_x are defined by

$$Gr=\frac{g\beta_T(T_w-T_\infty)x^3}{\nu^2}, \qquad Gc=\frac{g\beta_c(C_w-C_\infty)x^3}{\nu^2}, \qquad Re_x=\frac{u_w x}{\nu}. \quad (17)$$

The physical quantities of interest are the skin friction coefficient c_f , the local Nusselt number Nu_x , the local Sherwood number Sh respectively, which are defined as

$$c_f=\frac{\tau_w}{\rho u_w^2}, \qquad Nu_x=\frac{xq_w}{k(T_w-T_\infty)}, \qquad Sh=\frac{xj_w}{D_B(C_w-C_\infty)}, \quad (18)$$

where the surface shear stress τ_w , the surface heat flux q_w and the surface mass flux j_w are given by

$$\tau_w=\mu\left(\frac{\partial u}{\partial y}\right)_{y=0}, \qquad q_w=-\left(\left(k+\frac{16\sigma^* T_\infty^3}{3k^*}\right)\frac{\partial T}{\partial y}\right)\Big|_{y=0}, \qquad j_w=-D_B\left(\frac{\partial C}{\partial y}\right)_{y=0}. \quad (19)$$

Using the non-dimensional variables (10), we get

$$Re_x^{1/2}C_f=f''(0), \quad (20)$$

$$Nu_x Re_x^{-1/2}=-(1+\frac{4}{3}R_d)\theta'(0), \quad (21)$$

$$Sh\,Re_x^{-1/2}=-\phi'(0). \quad (22)$$

3. Results and discussion

Eqs. (11)-(13) subject to the boundary conditions (15) were solved numerically using the Runge–Kutta–Fehlberg method with a shooting technique for some values of the governing parameters. With neglecting the effects of Λ , $\lambda\theta$ and $\delta\phi$, the results for the skin friction coefficient $Re_x^{1/2}C_f$ are compared with those obtained by Mahapatra and Gupta [38], Nazar et al. [39], Ishak et al. [40], Hayat et al. [11] and Pal [41] for different values of in Table 1. The results show that the values obtained from the present numerical results are in very good agreement with those previously published results. The values of skin friction coefficient, local Nusselt number and local Sherwood number are tabulated in Table-2 for various values of thermal radiation parameter R_d , the constant magnetic/porous medium parameter Λ , the solutal buoyancy parameter δ , the Prandtl number Pr for both cases of assisting and opposing flows when ε = 1, Le = 5, λ = 1 and N_b = N_t =0.2. The values of the skin friction coefficient and the local Nusselt number increases when R_d and δ increase for assisting flows but for the opposing flow it shows a reverse behavior.

Table 1.

Values of $Re_x^{1/2}C_f$ for different values of ε in absence of buoyancy forces $\lambda\theta$, $\delta\phi$ and $\Lambda = 0$.

ε	Mahapatra and Gupta [33]	Nazar et al. [34]	Ishak et al. [35]	Hayat et al. [8]	Pal et al. [36]	Present results
0.1	–0.9694	–0.9694	–0.9694	–0.9694	–.96939	–0.9694
0.2	–0.9181	–0.9181	–0.9181	–0.9181	–0.91811	–0.9181
0.5	–0.6673	–0.6673	–0.6673	–0.6673	–0.66726	–0.6673
2.0	2.0175	2.0175	2.0175	2.0175	2.01750	2.0175
3.0	4.7293	4.7293	4.7293	4.7293	4.72928	4.7293

Table 2.

The effect of R_d , Λ , δ and Pr on the skin friction coefficient, local Nusselt number, local Sherwood number for both cases of assisting and opposing flows , when $\varepsilon = 1,\ Le = 5, \lambda = 1$ *and* $\mathrm{Pr} = 6.2$.

R_d	Λ	δ	Pr	**Assisting flow**			**Opposing flow**		
				$Re_x^{1/2}C_f$	$Nu_xRe_x^{-1/2}$	$ShRe_x^{-1/2}$	$Re_x^{1/2}C_f$	$Nu_xRe_x^{-1/2}$	$ShRe_x^{-1/2}$
0.5	1.5	1.0	6.2	0.5502	1.2987	1.7508	-0.5820	1.2120	1.6258
1.5				0.5682	1.2760	1.7018	-0.6018	1.1800	1.5790
3.0				0.5870	1.1583	1.6886	-0.6228	1.0637	1.5562
5.0				0.6036	1.0300	1.6459	-0.6408	0.9433	1.5211
0.5	0.0	1.0	6.2	0.6078	1.3047	1.7584	-0.6600	1.2010	1.6098
	1.5			0.5502	1.2987	1.7508	-0.5820	1.2120	1.6258
	3.0			0.5092	1.2940	1.7416	-0.5306	1.2183	1.6354
	4.0			0.4868	1.2917	1.7382	-0.5042	1.2217	1.6400
0.5	1.5	0.0	6.2	0.2950	1.2828	1.7192	-0.3042	1.2343	1.6576
		1.0		0.5502	1.2987	1.7508	-0.5820	1.2120	1.6258
		2.0		0.8012	1.3153	1.7722	-0.8690	1.1873	1.5916
		3.0		1.0470	1.3313	1.7946	-1.1685	1.1595	1.5514
0.5	1.5	1.0	0.03	0.6574	0.5617	1.8554	-0.6908	0.5660	1.6906
			1.0	0.6144	0.9407	1.7518	-0.6520	0.8637	1.6426
			6.2	0.5502	1.2987	1.7508	-0.5820	1.2120	1.6258
			10.0	0.5406	1.3290	1.7456	-0.5704	1.2658	1.6041

A similar effect on the skin friction coefficient is observed when Λ and Pr decrease. From this table, for assisting flows, the magnitude of the local Nusselt number increases by increasing δ and Pr . Clearly, there is the reverse behaviors for the opposing flows. A similar effect on the local Nusselt number is observed when Λ and R_d decrease. Moreover, the magnitude of the local Sherwood number increases by increasing δ for assisting flows. But for the opposing flow it shows a reverse behavior. A similar effect on the local Sherwood number is observed when Λ , R_d and decrease. The effect of Λ , λ, δ , ε , N_t , N_b , R_d , Pr and Le on the velocity profiles $f'(\eta)$ for both cases of assisting and opposing flows are illustrated in Figures 2–10, respectively. Figure-2 displays that for assisting flow the velocity $f'(\eta)$ decreases as Λ increases but for the opposing flow it shows a reverse behavior. Moreover, The boundary layer thickness is decreased by increasing Λ .The reason behind this phenomenon is that application of magnetic field to an electrically conducting fluid give rise to a resistive type force called the Lorentz force. This force has the tendency to slow down the motion of the fluid in the boundary layer.

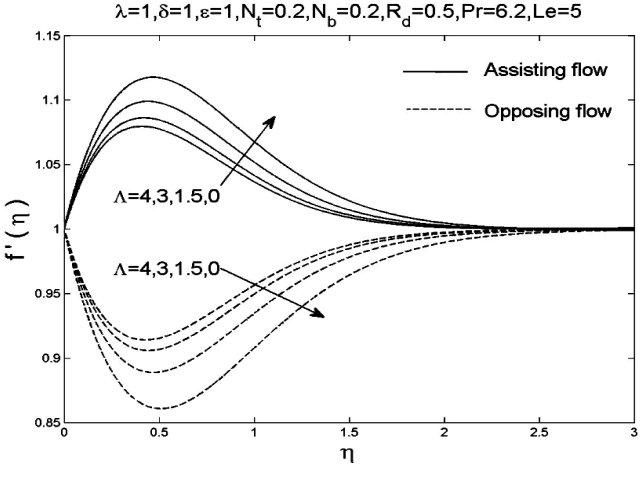

Fig. 2. The effect of the constant magnetic/porous medium parameter Λ on the velocity profiles $f'(\eta)$.

Figure-3 indicates the infuence of λ on the velocity profiles $f'(\eta)$. It was observed that for the assisting flow the velocity increases at the beginning until it achieves

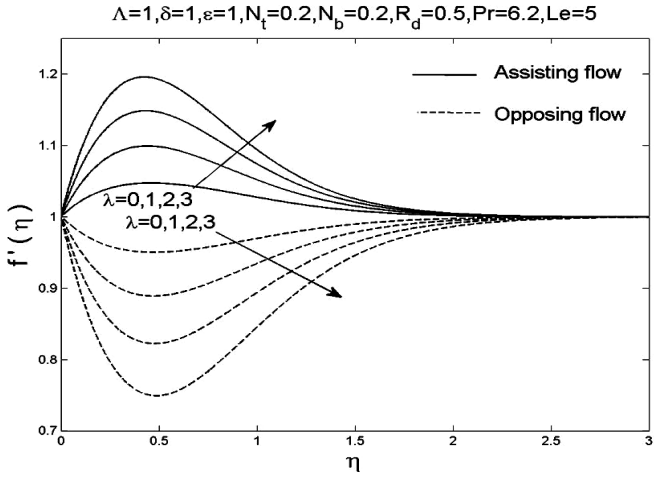

Fig. 3. The effect of the buoyancy parameter λ on the velocity profiles $f'(\eta)$.

a certain value, then decreases until the value becomes constant, that is unity, at outside the boundary layer. The results of velocity are noted to be more pronounced for large λ . This is because, large value of λ produces large buoyancy force which produces large kinetic energy. Then the energy is used to overcome a resistance along the flow. As a result, it decreases and becomes constant far away from the surface. Figure-4 showes the effects of δ on $f'(\eta)$. It can be seen from this Figure that δ has the similar behavior as in Figure-3. The variation of ε on $f'(\eta)$ is seen in Figure-5. It is noted that when ε >1, the flow has a boundary layer structure and the thickness of the boundary layer decreases with increase in ε .According to Mahapatra and Gupta [38], it can be explained as follows: for a fixed value of c corresponding to the stretching of the surface, an increase in a in relation to c (such that ε >1) implies an increase in straining motion near the stagnation region resulting in increased acceleration of the external stream, and this leads to thinning of the boundary layer with an increase in ε . Further, it is seen from Figure-5 that when ε < 1, the flow has an inverted boundary layer structure. It results from the fact that when ε < 1, the stretching velocity of the surface exceeds the velocity of the external stream Figure-6 display the effect of thermophoretic parameter N_t on the velocity profiles $f'(\eta)$. This Figure shows that the velocity of fluid increases in case of assisting flow by increasing N_t, however it is clear a reverse behavior for the opposing flow.

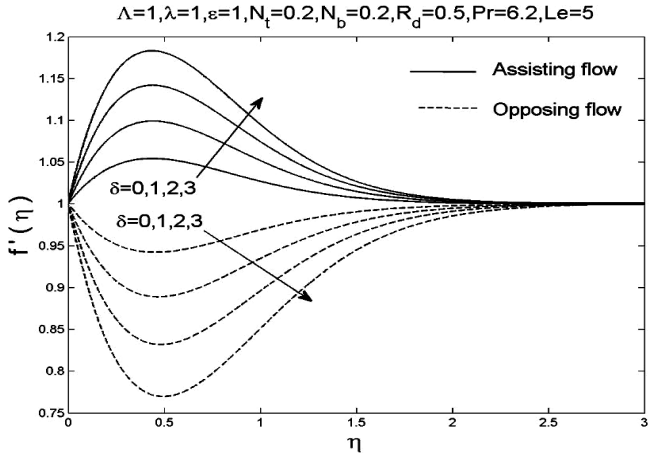

Fig. 4. The effect of the solute buoyancy parameter on the velocity profiles $f'(\eta)$.

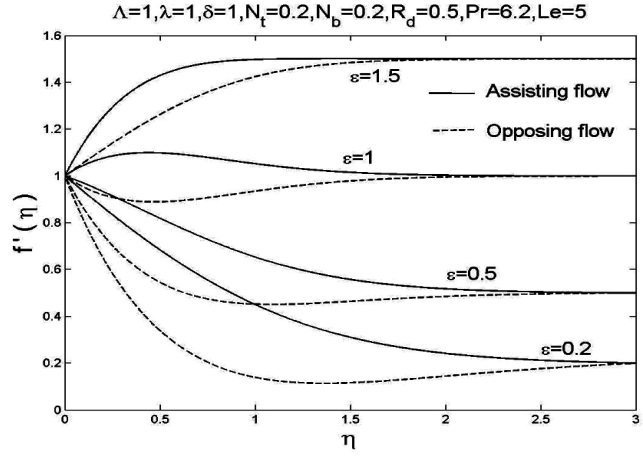

Fig. 5. The effect of the velocity ratio parameter on the velocity profiles $f'(\eta)$.

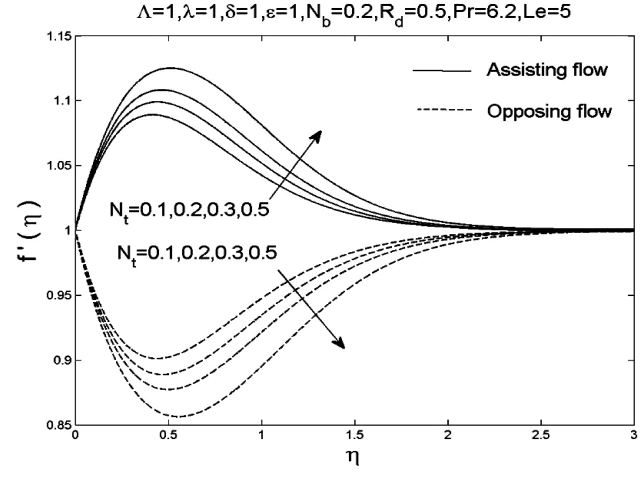

Fig. 6. The effect of the thermophoresis parameter N_t on the velocity profiles $f'(\eta)$.

Figure-7 indicates that the velocity of fluid decreases in case of assisting flow by increasing N_b but the reverse trend is noted in the opposing flow. Figure-8 also shows the effects of R_d on $f'(\eta)$. It can be seen from this Figure, that R_d has the similar behavior as in Figure-6

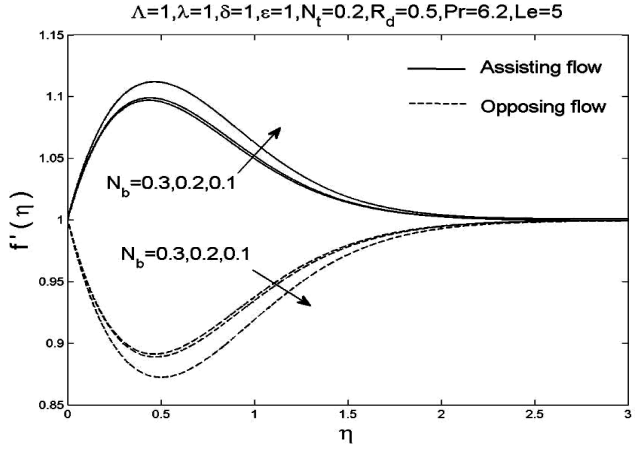

Fig. 7. The effect of the Brownian motion parameter N_b on the velocity profiles $f'(\eta)$.

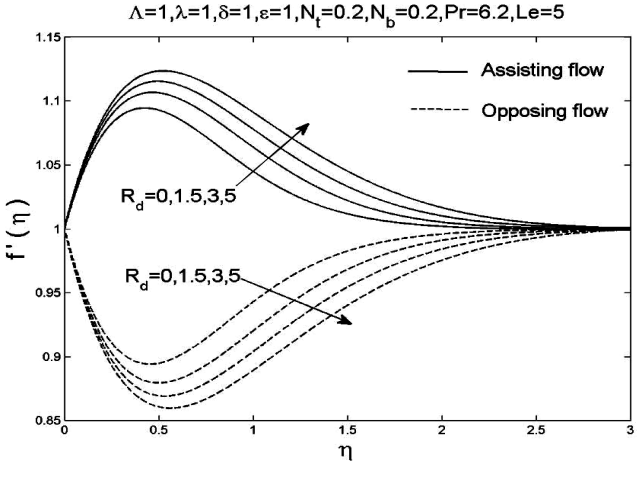

Fig. 8. The effect of the radiation parameter R_d on the velocity profiles $f'(\eta)$.

Figure-9 indicates that the velocity of fluid decreases in case of assisting flow by increasing Pr but the reverse trend is noted in the opposing flow. From Figure-10, it is observed that Le has the similar behavior as in Figure-9..

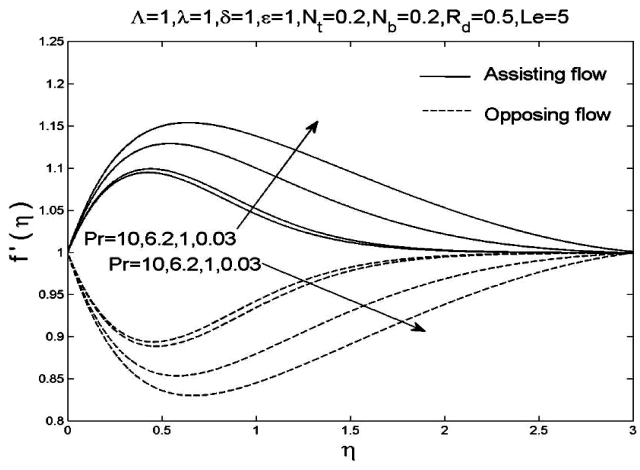

Fig. 9. The effect of the Prandtl number Pr on the velocity profiles $f'(\eta)$.

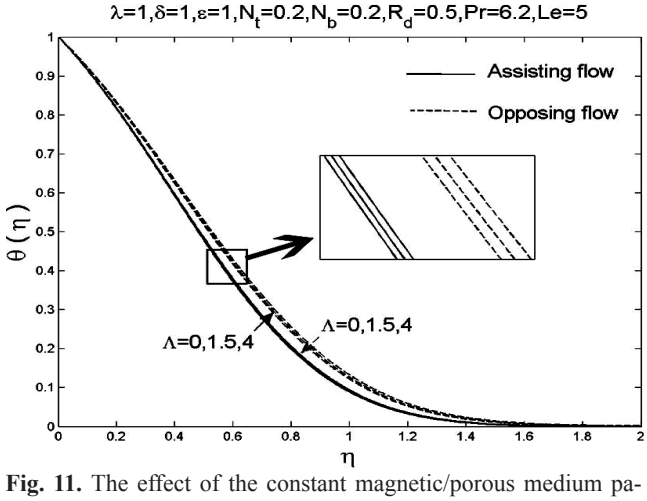

Fig. 11. The effect of the constant magnetic/porous medium parameter Λ on the temperature profiles, $\theta(\eta)$.

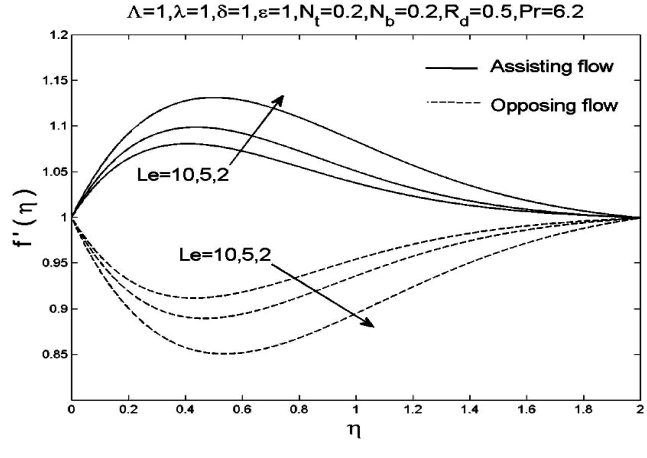

Fig. 10. The effect of the lewis number Le on the velocity profiles $f'(\eta)$.

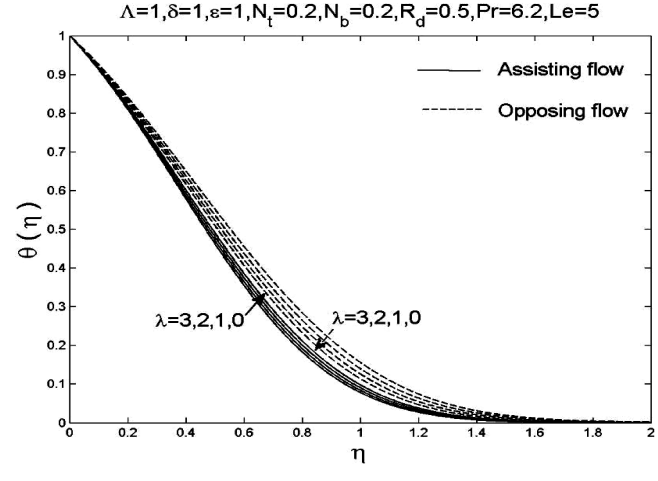

Fig. 12. The effect of the buoyancy parameter λ on the temperature profiles $\theta(\eta)$.

The effect of Λ, λ , δ , ε , N_t , N_b, R_d, Pr and Le on the temperature profiles $\theta(\eta)$ for both cases of assisting and opposing flows are illustrated in Figures 11–19, respectively. From Figure-11, it is observed that the temperature profiles $\theta(\eta)$ increases in case of assisting flow by increasing Λ but the reverse trend is noted in the opposing flow. Moreover, this increment in $\theta(\eta)$ is larger in case of an opposing flow. It can be seen from Figure-12 that for assisting flow the temperature components decrease with increase in the mixed convection parameter λ, but a reverse behaviar is observed for the opposing flow. Figure-13 indicates the effects of δ on $\theta(\eta)$. It can be seen from this Figure that δ has the similar behavior as in Figure-12. From Figure-14, it is observed that the temperature profiles $\theta(\eta)$ decrease in both cases of assisting and opposing flows by increasing ε. Besides, the thermal boundary layer decrease as ε increase in both cases.

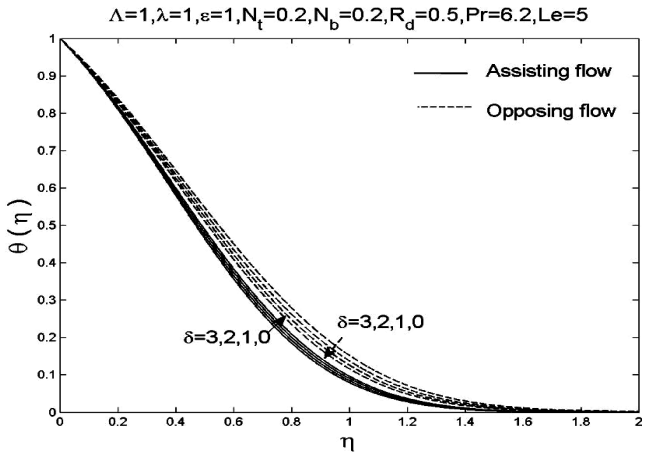

Fig. 13. The effect of the solutal buoyancy parameter δ on the temperature profiles $\theta(\eta)$.

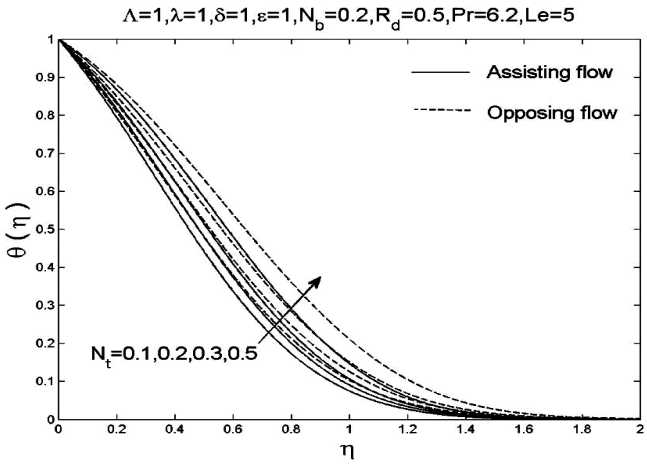

Fig. 15. The effect of the thermophoresis parameter N_t on the temperature profiles $\theta(\eta)$.

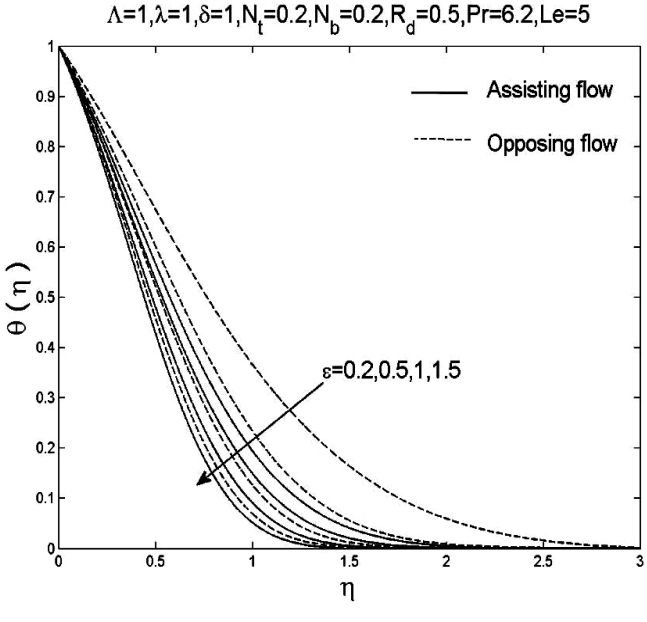

Fig. 14. The effect of the velocity ratio parameter ε on the temperature profiles $\theta(\eta)$.

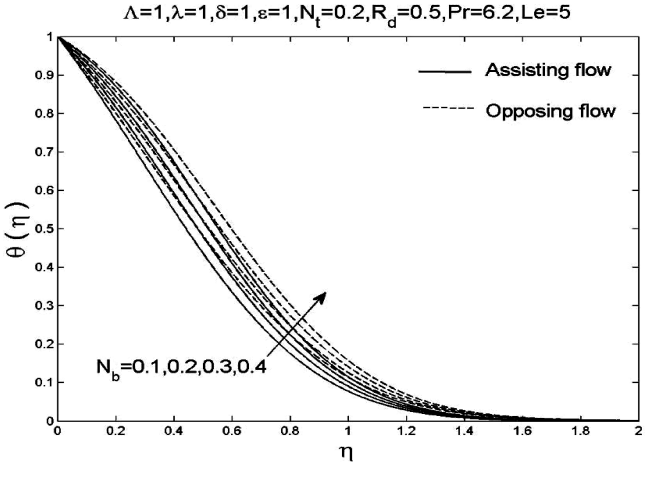

Fig. 16 The effect of the Brownian motion parameter N_b on the temperature profiles $\theta(\eta)$.

Figures-15 and 16 display the effect of thermophoretic parameter N_t on temperature profiles. It is to note that the temperature of the fluid increases with increase of N_t in both cases of assisting and opposing flows. Moreover, The boundary layer thickness is increased by increasing N_t.It can be seen from Figure-16 that N_b has the similar behavior as in Figure-15. From Figure-17, it is observed the temperature $\theta(\eta)$ increases by increasing R_d in both cases of assisting and opposing flows. It is observed that the increase of the radiation parameter R_d leads to an increase of the temperature profiles and to an increase of the boundary layer thickness. Therefore, higher values of R_d imply higher surface heat flux and thereby making the fluid become warmer. This enhances the effect of the thermal buoyancy of the driving body force due to mass density variations which are coupled to the temperature and, therefore, increasing the fluid velocity.

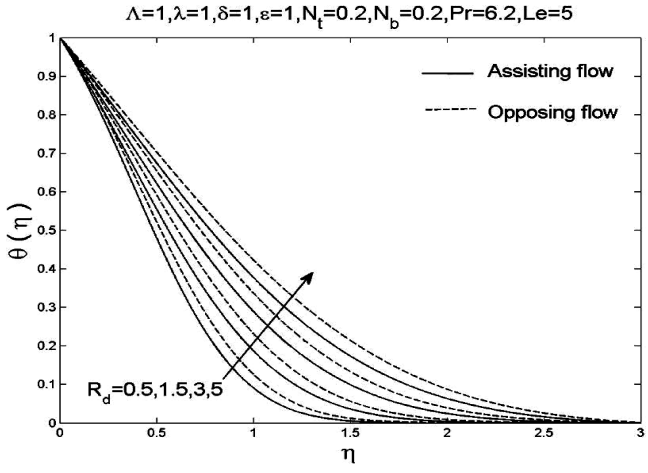

Fig. 17. The effect of the radiation parameter on the temperature profiles $\theta(\eta)$.

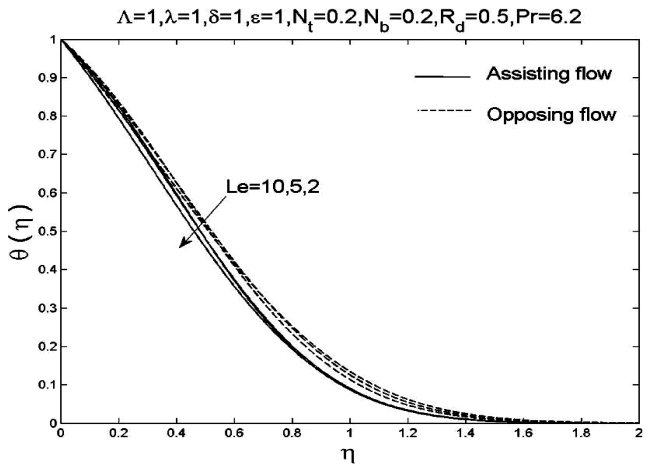

Fig. 19 . The effect of the lewis number Le on the temperature profiles $\theta(\eta)$.

Figure-18 shows that the thermal boundary layer thickness increases with decrease in the value of Pr which is associated with an increase in the wall temperature gradient and, hence, produces an increase in the surface heat transfer rate in both the cases of assisting and opposing flows. Further, the temperature θ decreases with the increase in Pr . The effects of thermal buoyancy force are more pronounced on dimensionless temperature for a fluid with a small Pr . for small values of Pr $(<<1)$, the fluid is highly conductive. Physically, if Pr increases, the thermal diffusivity decreases and this phenomenon leads to the decreasing of energy transfer ability that reduces the thermal boundary layer. Figure-19 displays that Le has the similar behavior as in Figure-18.

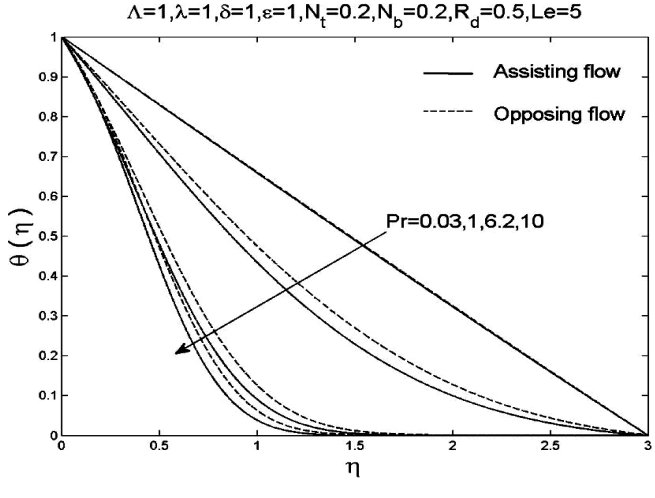

Fig. 18 . The effect of the Prandtl number Pr on the temperature profiles $\theta(\eta)$.

The variations in concentration with η for various values of Λ , λ , δ, ε , N_t , N_b and Le are shown in Figures 20–26, respectively. From Figure-20, it is observed that the concentration increases with increasing the value of the constant magnetic/porous medium parameter Λ for assisting flow and this trend is reversed for opposing flow. Figure-21 shows that the concentration decreases with increasing the value of thermal buoyancy parameter λ for assisting flow and this trend is reversed for opposing flow.

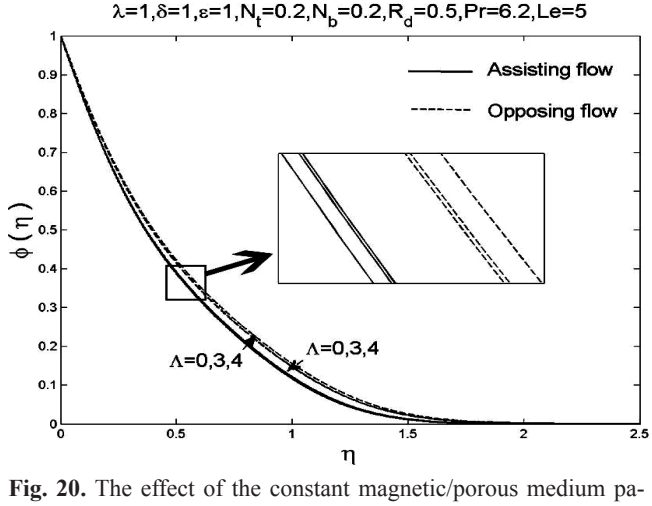

Fig. 20. The effect of the constant magnetic/porous medium parameter Λ on the concentration profiles $\phi(\eta)$.

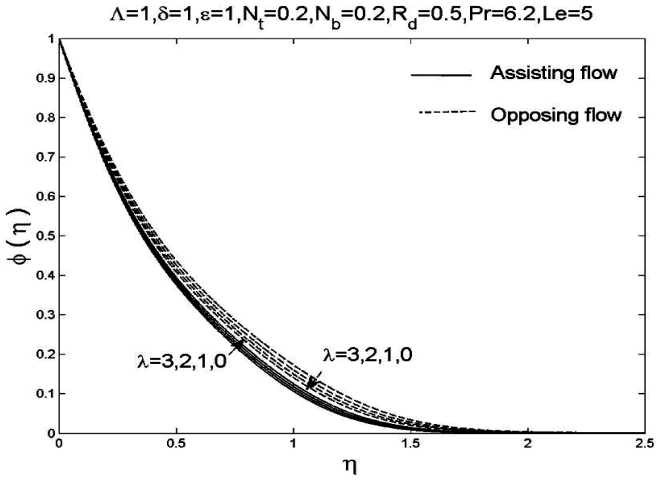

Fig. 21. The effect of the buoyancy parameter λ on the concentration profiles $\phi(\eta)$.

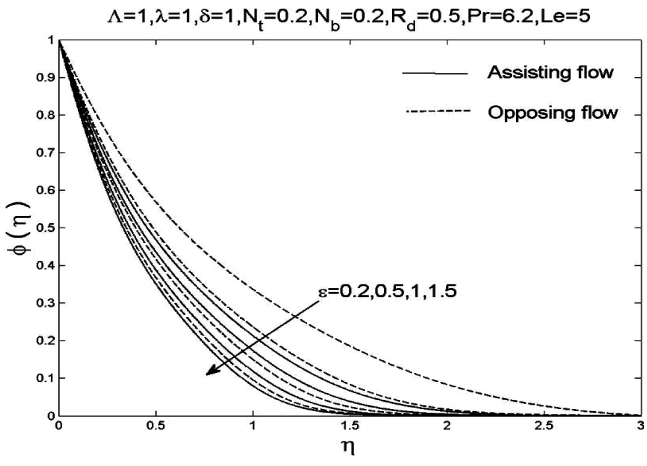

Fig. 23. The effect of the velocity ratio parameter ε on the concentration profiles $\phi(\eta)$.

Figure-22 displays that has the similar behavior as in Figure-21. From Figure-23, it is seen that the concentration decreases with increase in the values of ε for both of assisting and opposing flows

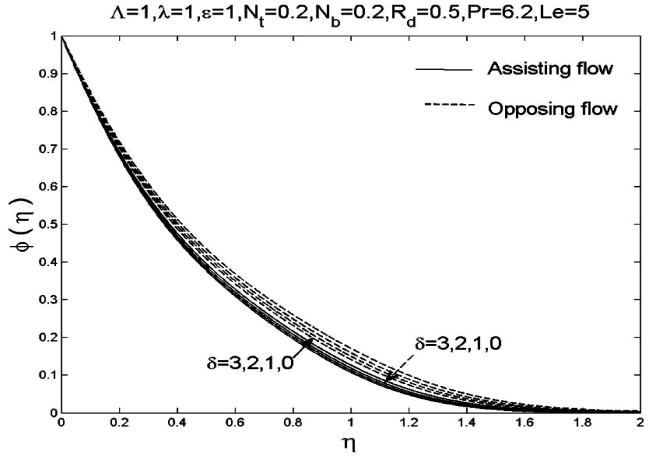

Fig. 22. The effect of the solutal buoyancy parameter δ on the concentration profiles $\phi(\eta)$.

Figure-24 displays the effect of thermophoretic parameter N_t on nanoparticle volume fraction profiles. It is to note that the nanoparticle volume fraction increases with increase of N_t We notice that, positive N_t indicates a cold surface, but is negative to a hot surface. For hot surfaces, thermophoresis tends to blow the nanoparticle volume fraction boundary layer away from the surface since a hot surface repels the sub-micron sized particles from it, thereby forming a relatively particle-free layer near the surface. Figure-25 illustrates the nanoparticle volume fraction profiles for various values of Brownian motion parameter, N_b Nanoparticle volume fraction decreases with increase of N_b .

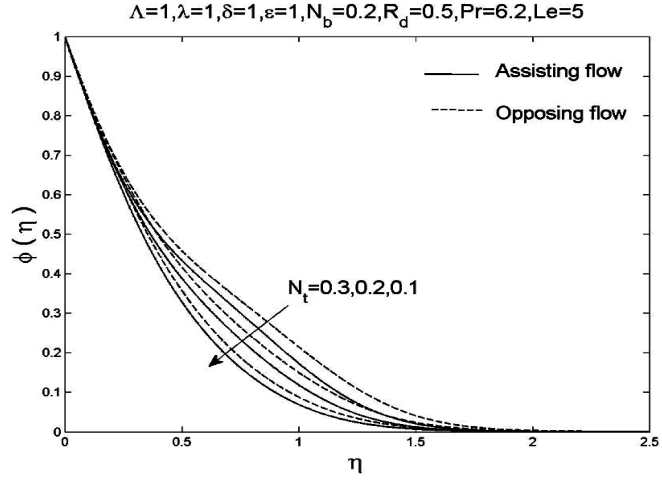

Fig. 24. The effect of the thermophoresis parameter N_t on the concentration profiles $\phi(\eta)$.

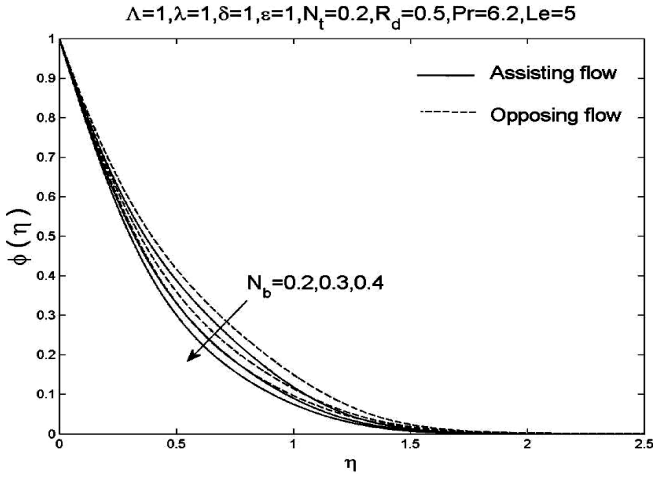

Fig. 25. The effect of the Brownian motion parameter N_b on the concentration profiles $\phi(\eta)$.

It is interesting to note that Brownian motion of nanoparticles at the molecular and nanoscale levels is a key nanoscale mechanism governing their thermal behavior. In nanofluid systems, due to the size of the nanoparticles Brownian motion takes place which can affect the heat transfer properties. As the particle size scale approaches to the nano-meter scale, the particle Brownian motion and its effect on the surrounding liquids play an important role in heat transfer. The behavior of Lewis number Le is shown in Figure-26. Since the larger values of Lewis number makes the molecular diffusivity smaller, therefore it decreases the concentration field for both of assisting and opposing flows.

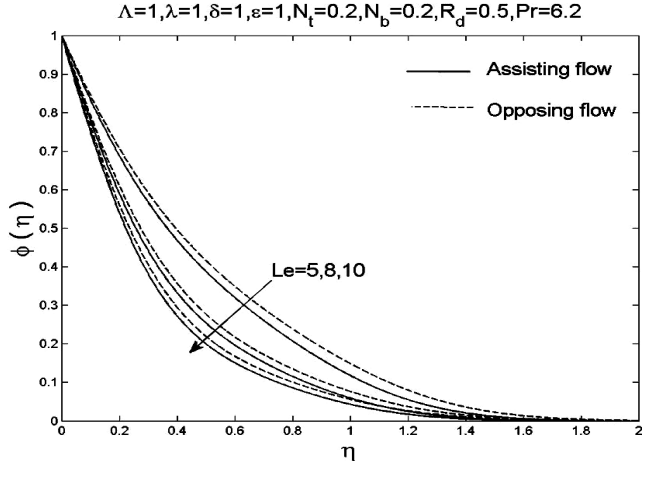

Fig. 26. The effect of the lewis number Le on the concentration profiles $\phi(\eta)$.

Figures 27-29 are prepared to present the effect of the Brownian motion parameter N_b and the thermophoresis parameter N_t on the skin friction coefficient $Re_x^{1/2}C_f$, the local Nusselt number $Nu_x Re_x^{-1/2}$ and the local Sherwood number $ShRe_x^{-1/2}$ in both cases of the assisting and opposing flows. From Figure-27, it is observed that the magnitude of skin friction coefficient increases with the increases in N_t and decreases in N_b . but for the opposing flow it shows a reverse behavior. Figure-28 displays that the local Nusselt number decreases with the increases in N_b and N_t in both cases of the assisting and opposing flows. Figure-29 shows that the local Sherwood number decrease with the thermophoresis parameter for lower Brownian parameter N_b and increase for larger values of N_b in both cases of the assisting and opposing flows.

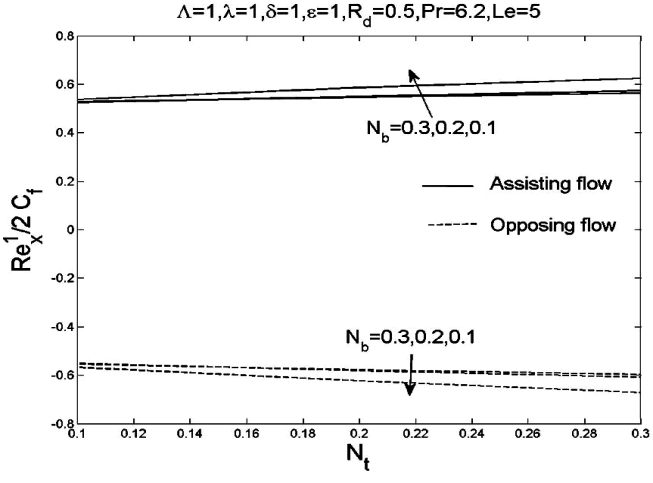

Fig. 27. The effect of the thermophoresis parameter N_t and N_b the Brownian motion parameter on the skin friction coefficient.

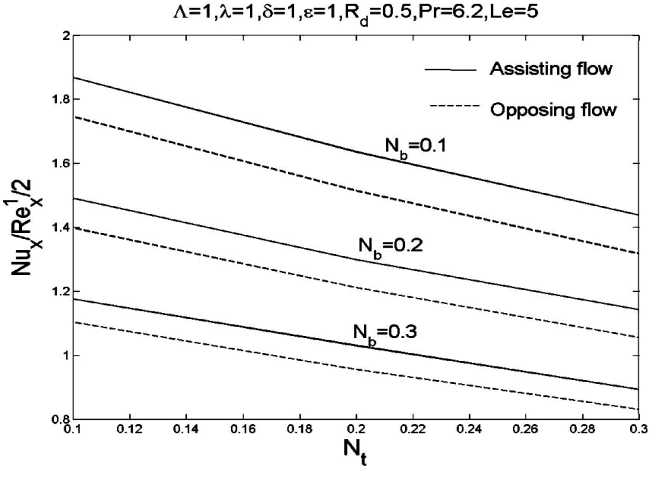

Fig. 28. The effect of the thermophoresis parameter N_t and N_b the Brownian motion parameter on the local Nusselt number .

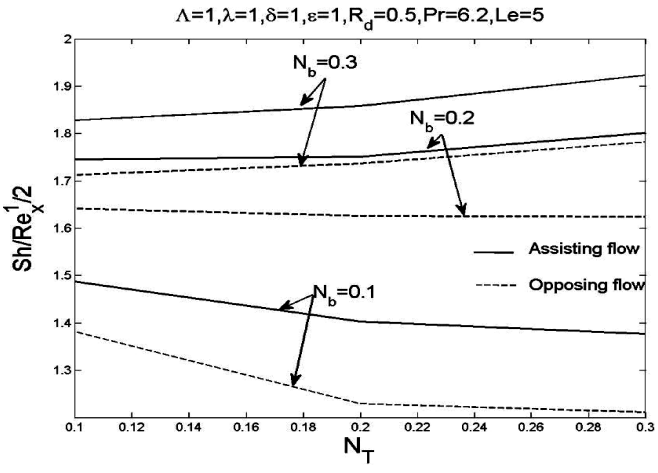

Fig. 29. The effect of the thermophoresis parameter N_t and the Brownian motion parameter N_b on the local Sherwood number

5. Conclusions

The two-dimensional mixed convection MHD boundary layer of stagnation-point flow over a stretching vertical plate in porous medium filled with a nanofluid and in the presence of thermal radiation was investigated. Both the effects of Brownian motion and thermophoresis are considered simultaneously. The governing partial differential equations were converted to ordinary differential equations using a suitable similarity transformation and were then solved numerically using the Runge–Kutta–Fehlberg method with a shooting technique. Similarity solution is presented which depends on the Brownian motion parameter N_b, the thermophoresis parameter N_t, the constant magnetic/porous medium parameter Λ, the mixed convection parameter λ, the solutal buoyancy parameter δ, The velocity ratio parameter ε, the Prandtl number Pr, the Lewis number Le and the radiation parameter R_d on the flow and heat and mass transfer characteristics. Finally, from the presented analysis, the following observations are noted.

•The velocity of fluid increases in case of assisting flow by decreasing Λ, N_b, Pr and Le but the opposite trend is noted in the opposing flows. A similar effect on the velocity is observed when λ, δ, N_t and R_d increases.

• The temperature increases by increasing N_b, N_t and R_d in both cases of buoyant assisting and opposing flows. A similar effect on the temperature is observed when Pr, Le and ε decreases.

• The concentration increases by increasing N_t in both cases of buoyant assisting and opposing flows. A similar effect on the temperature is observed when Le, and N_b decreases.

• The magnitude of skin friction coefficient increases with the increases in N_t and decreases in N_b. but for the opposing flow it shows a reverse behavior. Moreover, the local Nusselt number decreases with the increases in N_t and N_b in both cases of the assisting and opposing flows. Also, the local Sherwood number decrease with the thermophoresis parameter N_t for lower Brownian parameter N_b and increase for larger values of N_b.

• The volume fraction of nanoparticles is a key parameter for studying the effect of nanoparticles on flow fields and temperature distributions. It is interesting to note that the impact of thermophoresis particle deposition with Brownian motion have a substantial effect on the flow field and, thus, on the heat transfer and concentration rate from the sheet to the fluid.

Acknowledgment

This scientific product was extracted through a research project implemented from funding of research projects of Yasouj Branch, Islamic Azad University.

References

[1] K. Hiemenz, Die Grenzschicht an einem in den gleichformingen Flussigkeitsstrom einge-tauchten graden Kreiszylinder, Dinglers Polytech. J. 326 (1911) 321.

[2] F. Homann, Der Einfluss grosser Zahigkeit bei der Stromung um den Zylinder und um die Kugel, Z. Angew. Math. Mech. 16 (1936) 153.

[3] S. Dinarvand, on explicit, purely analytic solutions of off-centered stagnation flow towards a rotating disc by means of HAM, Nonlinear Anal. Real World Appl. 11 (2010) 3389.

[4] D. A. Nield, A. Bejan, Convection in Porous Media, third ed., Springer, New York, (2006).

[5] D. B. Ingham, I. Pop (Eds.), Transport Phenomena in Porous Media, Vol. II 2002, Pergamon, Oxford, (1998).

[6] D. B. Ingham, I. Pop (Eds.), Transport Phenomena in Porous Media, Vol. III, Elsevier, Oxford, (2005).

[7] A. Bejan, I. Dincer, S. Lorente, A.F. Miguel, A.H. Reis, Porous and Complex Flow Structures in Modern Technologies, Springer, New York, (2004).
[8] M.C. Ece, Free convection flow about a cone under mixed thermal boundary conditions and a magnetic field, Appl. Math. Model. 29 (2005) 1121.
[9] S. Dinarvand, A. Doosthoseini, E. Doosthoseini, M. M. Rashidi , Series solutions for unsteady laminar MHD flow near forward stagnation point of an impulsively rotating and translating sphere in presence of buoyancy forces, Nonlinear Anal. Real World Appl. 11 (2010) 1159¬.
[10] S. Dinarvand, The laminar free-convection boundary-layer flows about a heated and rotating down-pointing vertical cone in the presence of a transverse magnetic field, Int. J. Numer. Meth. Fluids 67 (2011) 2141.
[11] T. Z. Hayat, I. Pop, S. Asghar, Effects of radiation and magnetic field on the mixed convection stagnation-point flow over a vertical stretching sheet in a porous medium, International Journal of Heat and Mass Transfer, 53 (2010) 466.
[12] K. Das, Impact of thermal radiation on MHD slip flow over a flat plate with variable fluid properties. Heat and Mass Transf. 48 (2011) 1.
[13] S.U.S. Choi, Enhancing thermal conductivity of fluids with nanoparticle, in: D.A. Siginer, H.P. Wang (Eds.), Developments and Applications of Non-Newtonian Flows, ASME FED, 231/66 (1995) 99.
[14] S. U. S. Choi, Z. G. Zhang, W. Yu, F. E. Lockwood, E. A. Grulke, Anomalously thermal conductivity enhancement in nanotube suspensions, Appl. Phys. Lett. 79 (2001) 2252.
[15] H. Kang, S.H. Kim, J. M. Oh, Estimation of Thermal Conductivity of Nanofluid using Experimental Effective Particle Volume, Exp. Heat Transf. 19 (2006) 181.
[16] V. Velagapudi, R. K. Konijeti, C. S. K. Aduru, Empirical Correlation to Predict Thermophysical and Heat Transfer Characteristics of Nanofluids, Thermal Sci. 12 (2008) 27.
[17] A. Turgut, Tavman, I., Chirtoc, M., Sauter, C., Tavman, S., Thermal Conductivity and Viscosity Measurements of Water-Based TiO_2 Nanofluids, Int. J. Thermophys 30 (2009) 1213.
[18] V.Y. Rudyak, Belkin, A. A., E. A.Tomilina, On the Thermal Conductivity of Nanofluids, Technical Physics Letters 36 (2010) 660.
[19] C. Murugesan, S. Sivan, Limits for Thermal Conductivity of Nanofluids, Thermal Sci. 14 (2010) 65.
[20] R.J. Tiwari, M.K. Das, Heat transfer augmentation in two-sided lid-driven differentially heated square cavity utilizing nanofluids, Int. J. Heat Mass Transfer, 50 (2007) 2002.
[21] A. K. Nayak, K. Singh, P. P. Kulkarni, Measurement of Volumetric Thermal Expansion Coefficient of Various Nanofluids, Technical Physics Letters, 36 (2010) 696.
[22] S. Ahmad, I. Pop, Mixed convection boundary layer flow from a vertical flat plate embedded in a porous medium filled with nanofluids, Int. Comm. Heat Mass Transfer, 37 (2010) 987.
[23] S. Dinarvand, A. Abbassi, R. Hosseini, I. Pop, homotopy analysis method for mixed convective boundary layer flow of a nanofluid over a vertical circular cylinder, Thermal Science, 19 (2015) 549.
[24] J. A. Gbadeyan, M.A. Olanrewaju, P.O. Olanrewaju, Boundary Layer Flow of a Nanofluid Past a Stretching Sheet with a Convective Boundary Condition in the Presence of Magnetic Field and Thermal Radiation, Australian Journal of Basic and Applied Sciences, 5 (2011) 1323.
[25] S. Dinarvand, R. Hosseini, E. Damangir, I. Pop, Series solutions for steady three-dimensional stagnation point flow of a nanofluid past a circular cylinder with sinusoidal radius variation, Meccanica, 48 (2013) 643.
[26] A. Chamkha, A. Al-Mudhaf, I. Pop, Effect of heat generation or absorption on thermophoretic free convection boundary layer from a vertical flat plate embedded in a porous medium, Int. Commun. Heat Mass Transfer, 33 (2006) 1096.
[27] S. L. Goren, The role of thermophoresis in laminar flow of a viscous and incompressible fluid, J. Colloid. Interface Sci. 61(1977) 77.
[28] A.J. Chamkha, I. Pop, Effects of thermophoresis particle deposition in free convection boundary layer from a vertical flat plate embedded in a porous medium, Int. Commun. Heat Mass Transfer, 31(2004) 421.
[29] M.S. Aslam, M.M. Rahman, M.A. Sattar, Effects of variable suction and thermophoresis on steady MHD combined free-forced connective heat and mass transfer flow over a semi-infinite permeable inclined plate in the presence of thermal radiation, Int. J. Thermal. Sci. 47 (2008) 758.
[30] R. Kandasamya, Muhaimina, I. Hashim, Ruhailaa, Thermophoresis and chemical reaction effects on non-Darcy mixed convective heat and mass transfer past a porous wedge with variable viscosity in the presence of suction or injection, Nuclear Eng. Design, 238 (2008) 2699.
[31] T. Gsosan, R. Pop, I. Pop, Thermophoretic deposition of particles in fully developed mixed convection flow

in a parallel-plate vertical channel, Heat Mass Transfer 45 (2009) 503.

[32] K. Das, Effects of thermophoresis and thermal radiation on MHD mixed convective heat and mass transfer flow, Africa Mathematica 24 (2012) 511.

[33] A. V. Kuznetsov, D. A. Nield, Natural convective boundary-layer flow of a nanofluid past a vertical plate, Int. J. Thermal Sci. 49 (2010) 243.

[34] D.A. Nield, A.V. Kuznetsov, The Cheng-Minkowycz problem for natural convective boundary layer flow in a porous medium saturated by a nanofluid, Int. J. Heat Mass Transfer 52 (2009) 5792.

[35] P. Cheng, W.J. Minkowycz, Free convection about a vertical flat plate embedded in a porous medium with application to heat transfer from a dike, J. Geophys. Res. 82 (1977) 2040.

[36] J. Buongiorno, Convective transport in nanofluids, J. Heat Transfer, 128 (2006) 240.

[37] W. A. Khan, I. Pop, Boundary-layer flow of a nanofluid past a stretching sheet, Int. J. Heat Mass Transfer 53 (2010) 2477.

[38] T. R. Mahapatra, A.S. Gupta, Heat transfer in stagnation-point towards a stretching sheet, Heat Mass Transfer, 38 (2002) 517.

[39] R. Nazar, N. Amin, D. Flip, I. Pop, Unsteady boundary layer flow in the region of the stagnation point on a stretching sheet, Int. J. Eng. Sci. 42 (2004) 1241.

[40] A. Ishak, R. Nazar, I. Pop, Mixed convection boundary layers in the stagnation-point flow toward a stretching vertical sheet, Mechanica 41 (2006) 509.

[41] D. Pal, Heat and mass transfer in stagnation-point flow towards a stretching surface in the presence of buoyancy force and thermal radiation, Mechanica 44 (2009) 145.